Thermal impedance of SiGe HBTs: Characterization and modeling

Xiaodi Jin[1], Guangsheng Liang[1], Yves Zimmermann[1], Gerhard Fischer[2], Christoph Weimer[1], Mario Krattenmacher[1], Yaxin Zhang[1], Michael Schröter[1], *Senior Member IEEE*

[1]Chair for Electron Devices and Integrated Circuits, TU Dresden, 01069 Dresden, Germany

[2]IHP - Leibniz-Institut für innovative Mikroelektronik, 15236 Frankfurt (Oder), Germany

***Abstract* - Electro-thermal characterization of SiGe HBTs was performed for different operating points. Small-signal simulations with a single-pole and various multi-pole thermal networks are compared with measured data over a wide frequency range. The results show that nodal and recursive thermal networks are unable to match the measured phase of the thermal impedance Z_{th}, while Foster, Cauer and Cauer-type recursive thermal networks are more accurate and flexible for modeling Z_{th}. Furthermore, a guide for the usage of different networks upon the phase of Z_{th} is provided.**

***Index Terms* - SiGe HBT, thermal impedance, characterization, thermal networks, Foster, Cauer, recursive.**

I. INTRODUCTION

Small-signal related model parameters for modern SiGe HBTs are usually extracted at frequencies above 1 GHz, where the impact of dynamic self-heating (SH) is assumed to be negligible and only static SH affects the electrical behaviour. This is confirmed from measurement shown in Fig. 1: above 1 GHz the capacitances extracted from measured *Y*-parameters become frequency independent. Therefore, the investigation of dynamic SH needs to be focused on the frequencies below 1 GHz, at which circuits for, e.g., the Internet-of-Things [1], wireless sensor networks (WSN) [2] and baseband processing [3] operate.

Dynamic SH is generally described in a compact model by a thermal sub-circuit. The mainstream compact models for SiGe HBTs, such as HICUM [4], MEXTRAM [5], VBIC [6], utilize a single-pole network consisting of a thermal resistance in parallel to a thermal capacitance. The simulated *Y*-parameters using HICUM/L2 with its single-pole thermal network show an acceptable agreement for Mag(Y_{12}) at frequencies above 100 MHz, but fail to represent the measurements at lower frequencies and for Y_{22} as shown in Fig. 2. Especially at high current densities, where SH is strong, the deviation is more significant. At frequencies below 1 MHz, the modeled Mag(Y_{12}) underestimates the measured data, whereas above 1 MHz up to around 100 MHz an overestimation is observed. Similar discrepancies can also be observed for the phase of Y_{12} and for Y_{22}. Therefore, the accuracy of a single-pole thermal network is insufficient at frequencies where dynamic SH is relevant.

Thermal compact modeling has been investigated in previous works [7-9]. In [7], a recursive thermal network was preferred due to lower number of parameters. In [8, 9], results of a Cauer thermal network were compared to measurements with good agreement, while its parameters were calculated from an analytical equation using known geometries and material parameters.

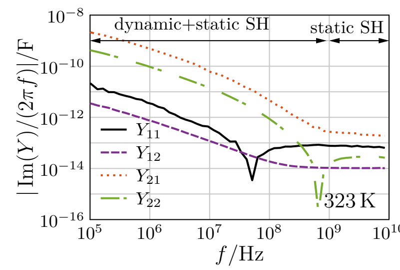

Fig. 1. Frequency dependence of the absolute value of the imaginary part of *Y* parameters normalized to the frequency at V_{BE} = 0.94 V and V_{CE} = 0.75 V from measured SiGe HBTs.

This work shows that recursive and nodal thermal networks fail to model the Z_{th} when its phase approaches -90°. In addition, single-pole, nodal, recursive, Foster, Cauer, and Cauer-type recursive thermal networks are parameterized based on measured thermal impedance data instead of relying on analytical calculations only. The limitation of single-pole network for frequency range is discussed. Furthermore, the trade-off between modeling accuracy and number of poles is investigated. After implementing the Foster, Cauer and Cauer-type recursive thermal networks into HICUM/L2, the simulated *Y*-parameters are compared with measured data for different bias points. Finally, a guide for chosing the thermal network is given.

II. INVESTIGATED PROCESS TECHNOLOGY AND DUT

A SiGe HBT fabricated with the SG13G2 technology from IHP was investigated. The standard process version [10] features f_T/f_{MAX} values of 300/500 GHz at room temperature (RT). The investigated transistor has a CEB contact configuration consisting of four parallel unit cells each with an emitter window area of 0.12 µm x 0.95 µm.

III. MEASUREMENT SETUP

A Süss probe station PA200 was used for the measurements over a temperature range from 298 K to 348 K. Bias dependent S-parameters were measured using a HP 4142 for DC voltage supply and a R&S ZNB8 with a frequency range from 9 kHz to 8.5 GHz, using SOLT calibration and Open-Short deembedding. Python based software (PyLab) was used to control the ZNB8 and for data acquisition [11]. The bias Tee limited the lower bound of the measurement frequency to 100 kHz.

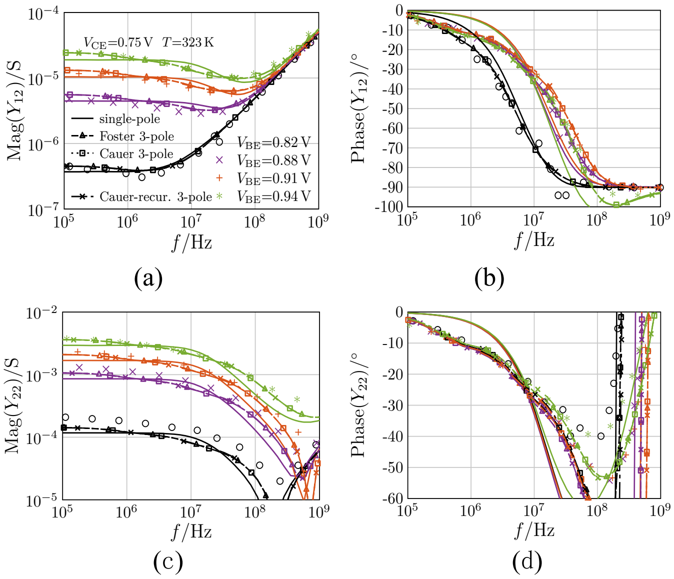

Fig. 2. (a) (c) Magnitude and (b) (d) phase of Y_{12} and Y_{22} for different V_{BE} of (0.82, 0.88, 0.91, 0.94) V at V_{CE} = 0.75 V. Comparison between HICUM/L2 results (lines) with Foster, Cauer, Cauer-type recursive, and single-pole thermal networks and measured data (symbols). The results from Foster, Cauer, and Cauer-type recursive thermal networks overlap each other. The legend in (a) also applies to (b)-(d).

IV. Characterization

A. Y-parameters

Compared to Y_{11} and Y_{21}, dynamic SH effects are more visible for Y_{12} and Y_{22} [9]. Hence, the magnitude and phase of Y_{12} and Y_{22} were characterized in detail and are shown in Fig. 2. The four chosen bias points correspond to (J_C/(mA/µm^2), f_T/GHz) = (4.1, 209), (13.2, 215), (19.7, 321), (26.8, 214), while peak-f_T (= 326 GHz) occurs at i.e. 17.4 mA/µm^2. An ambient temperature of 323 K instead of 298 K was chosen, because the applied extraction method for Z_{th} (see (2)) requires the derivative of I_C versus T (c.f. [12-14]).

As depicted in Fig. 2, at low frequencies the magnitude of Y_{12} and Y_{22} decreases with increasing frequency, because the dynamic SH weakens and thus the real part of Y_{12} and Y_{22} decreases. At higher but not too high frequencies, the magnitudes increase linearly with frequency due to the dominating imaginary parts so that one can write the approximation,

$$\boldsymbol{Y} = \boldsymbol{G} + \mathrm{j} \cdot 2 \cdot \pi \cdot \boldsymbol{f} \cdot \boldsymbol{C} . \tag{1}$$

From 0.1 MHz to 100 MHz the reduction of the magnitude of Y_{12} at higher V_{BE} is more visible than at lower V_{BE} (c.f. Fig. 2(a)). At different bias, the phase trends are very similar showing a decrease with increasing frequency (c.f. Fig. 2(b) and (d)).

B. Thermal impedance

There are different methods for extracting Z_{th}: from *Y*-parameters [12-14] or from *H*-parameters [15]. In this work, a widely used *Y*-parameter method [12-14] is applied which gives

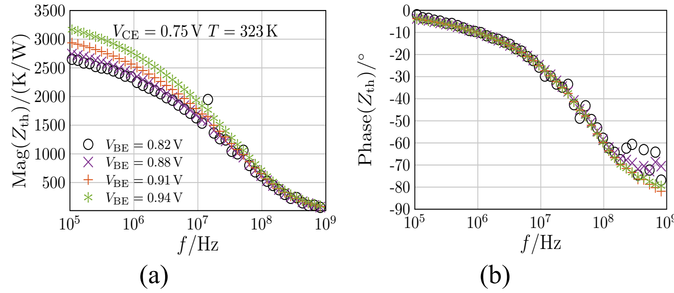

Fig. 3. Extracted (a) magnitude and (b) phase of Z_{th} for different V_{BE} = (0.82, 0.88, 0.91, 0.94) V at V_{CE} = 0.75 V. The legend in (a) also applies to (b).

$$\boldsymbol{Z}_{th} = \frac{\boldsymbol{Y}_{22} - \boldsymbol{Y}_{22,0}}{\boldsymbol{c}_m(\boldsymbol{I}_C + \boldsymbol{V}_{CE}\boldsymbol{Y}_{22} + \boldsymbol{V}_{BE}\boldsymbol{Y}_{12})(1+\boldsymbol{b})} . \tag{2}$$

Here, $Y_{22,0}$ indicates the isothermal Y_{22} that is obtained at higher frequencies where the impact of dynamic SH on electrical behaviour becomes negligible, c_m is the derivative of I_C w.r.t. *T*, and *b* is given by

$$\boldsymbol{b} = \left.\frac{\boldsymbol{P}}{\boldsymbol{Z}_{th}}\frac{\partial \boldsymbol{Z}_{th}}{\partial \boldsymbol{P}}\right|_{\boldsymbol{T}_{amb}} . \tag{3}$$

For simplification, *b* is set as 0 here. The magnitude and phase of the extracted Z_{th} are shown in Fig. 3. The magnitude of Z_{th} drops to zero with increasing frequency, i.e. the dynamic SH cannot follow the frequency. The phase of Z_{th} decreases to around -80°, indicating an increasing dominance of the imaginary part versus the real part.

V. Compact Thermal Modeling

A. Thermal networks

The investigated equivalent circuits are depicted in Fig. 4 [16-19]. The single-pole network has two parameters. The Foster and Cauer networks both have 2*n* parameters, with *n* being the number of poles. The nodal network has three, and the recursive network has five, and the Cauer-type recursive network has four parameters, i.e., their number of parameters is independent on the number of poles. The *k* coefficients should be given physically as $k_r < 1$ and $k_c > 1$ [20]. When the coefficients k_r and k_c of recursive network are set to one, the form of this network simplifies to that of nodal network.

B. Comparison of thermal impedance models

The parameters of the above mentioned thermal networks are extracted from measured Z_{th} data using (2). The multi-pole networks utilizing eight poles are first compared to measurements. Although, for circuit design, eight poles are impractical due to the large number of parameters and nodes, they provide the most accurate description and are thus used here as reference. According to the comparison shown in Fig. 5, the Foster, Cauer and Cauer-type recursive thermal networks agree very well with the measured magnitude and phase of Z_{th}, whereas other

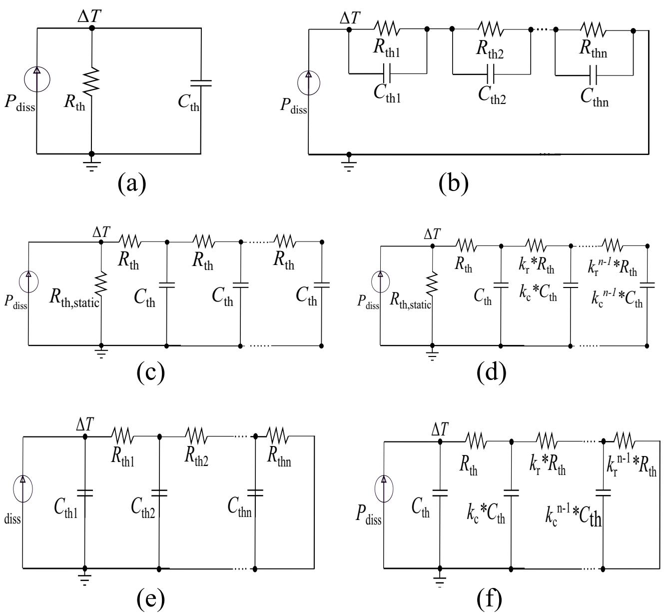

Fig. 4. Equivalent circuits of (a) single-pole, (b) Foster, (c) nodal, (d) recursive, (e) Cauer, and (f) Cauer-type recursive thermal networks for modeling thermal effects.

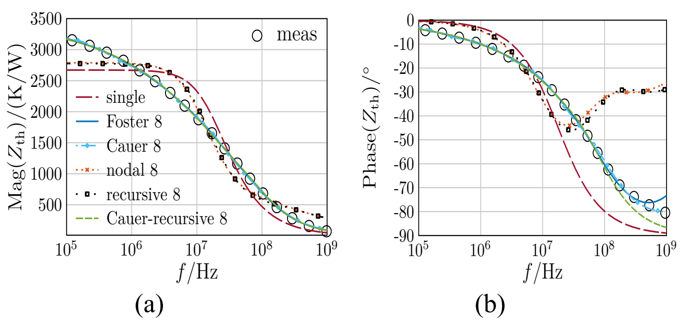

Fig. 5. Comparison of (a) magnitude and (b) phase of Z_{th} between thermal networks (lines) shown in Fig. 4 and measured values (symbols) with (V_{BE}, V_{CE}) = (0.94 V, 0.75 V) at 323 K.

multi-pole networks are unable to reach the measured phase at high frequencies. In [17], the recursive network showed good agreement because the phase of Z_{th} stayed above -45°. The phase shift can be qualitatively explained by considering the different spread of the heat flux into the substrate. A sufficiently small enclosure of the heating area by the DTI causes less spread of the heat flux so that it can respond faster to changes in heat generation. A faster response corresponds to a smaller phase shift.

In [17], the Foster network also shows reasonable agreement with the measured data although using more parameters than the recursive network. According to results in Fig. 5, the Foster, Cauer and Cauer-type recursive networks are more flexible (than the nodal and recursive networks) to model the thermal impedance of HBTs with different isolation schemes.

A smaller number of poles is preferred for reducing the number of model parameters. Therefore, the Foster, Cauer and Cauer-type recursive networks with a different number of poles are compared to measured data for finding the minimal

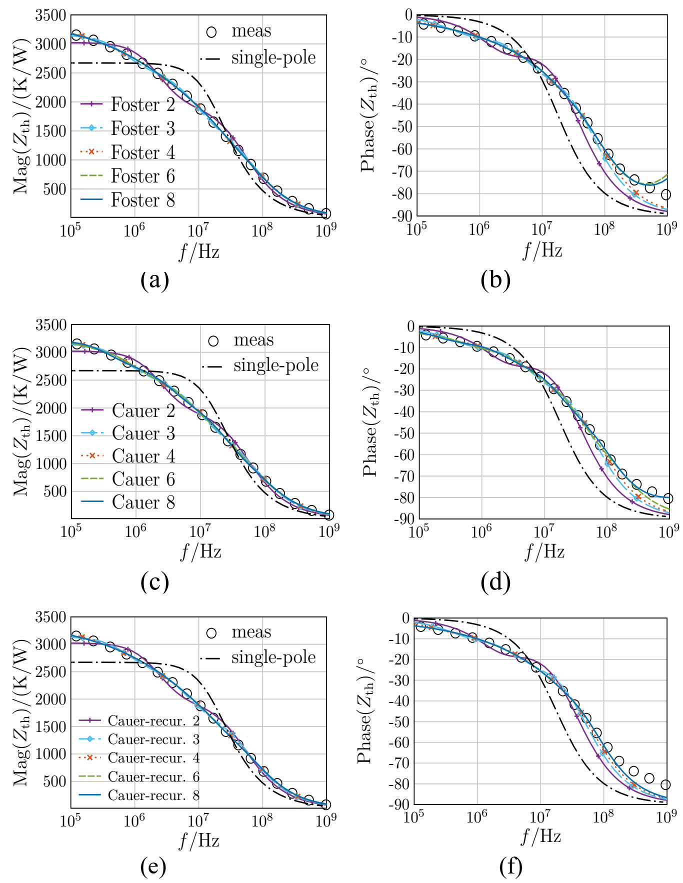

Fig. 6. Comparison of (a), (c), (e) magnitude and (b), (d), (f) phase of Z_{th} between Foster, Cauer, and Cauer-type recursive thermal networks (lines) with pole number of 2, 3, 4, 6, 8 and measured values (symbols) at V_{BE} = 0.94 V and V_{CE} = 0.75 V for T = 323 K. The results of the single-pole network are also shown.

necessary number of poles that still provide acceptable accuracy.

The investigated pole numbers are 2, 3, 4, 6, and 8. As shown in Fig. 6, the Foster, Cauer and Cauer-type recursive networks with three poles already yield an agreement that is comparable to that with 8 poles. The 2-pole network shows also a reasonable agreement in both magnitude and phase with some wiggles though.Even when using the most compact Foster, Cauer, or Cauer-type recursive network, i.e., $n = 2$, still four parameters to achieve reasonable agreement are required. For practical use, it is necessary to find a trade-off between accuracy, computation time, and ease of parameter extraction. Therefore, the single-pole model, which has the lowest number of parameters, is compared with measured data. The model parameters of the single-pole thermal network are extracted over different frequency ranges in order to determine a valid extraction frequency range. The comparison is given in Fig. 7. Good agreement for the magnitude can be achieved down to 10 MHz (see green short dashed lines), whereas the phase shows deviations already at 100 MHz (c.f. blue long dashed lines). This makes the single-pole network inaccurate below 100 MHz. Enlarging the extraction frequency range does not

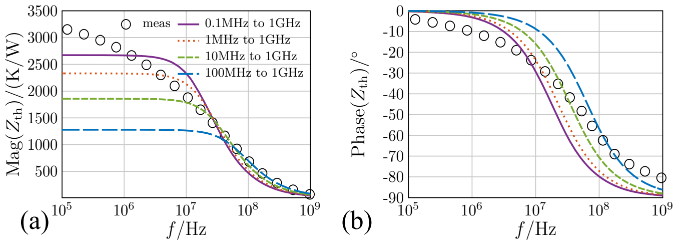

Fig. 7. Comparison of (a) magnitude and (b) phase of Z_{th} between single-pole thermal network and measured values at V_{BE} = 0.94 V and V_{CE} = 0.75 V for T = 323 K. The legends indicate that model parameters of single-pole thermal network were extracted from different frequency ranges.

improve the agreement, because least square optimization targets to achieve minimal deviations over the entire extracted frequency range. As a result, the model values obtained over a limited target frequency range from 100 MHz to 1 GHz show better agreement in the phase than using the range of 0.1 MHz to 1 GHz. In any case, using a single-pole network, there is no perfect fit to capture the wide frequency band.

C. Comparison of Y-parameters

The Foster, Cauer and Cauer-recursive thermal networks show good agreement with Z_{th} measurements. Here, with extracted model parameters, the simulated *Y*-parameters from HICUM/L2 with three-pole Foster, Cauer, and Cauer-recursive thermal networks and with the single-pole thermal network are compared in Fig. 2 with measurements. As expected, the simulated *Y*-parameters with Foster, Cauer, and Cauer-type recursive thermal networks show much better agreement than the single-pole thermal network, especially at high current densities where SH is more pronounced.

VI. Summary and Conclusions

Accurate modeling for the thermal impedance is required for HBTs and circuits operating at low frequencies. Application of the single-pole thermal network, as implemented in all standard HBT compact models, only shows good agreement above about 100 MHz. Below that frequency deviations are observed in the thermal impedance as well in *Y*-parameters. Five multi-pole thermal networks were compared here with measurements. Nodal and recursive networks show good agreement with measured Z_{th} as long as the measured phase of Z_{th} remains above about -55°~-45°, whereas Foster, Cauer, and Cauer-type recursive networks describe the frequency dependence of the phase accurately below and above mentioned values. Simulation results based on HICUM/L2 using a Foster, Cauer, or Cauer-recursive network with three poles agree with measured *Y*-parameters reasonably well down to at least 100 kHz. Choice and accuracy of the thermal network depends though on the device thermal propoties and isolation scheme, i.e., with and without DTI, as well as its location. The usage of different thermal networks is summarized in Table 1.

Acknowledgments

This work has been partially funded by the German National Science Foundation (DFG grant SCHR695/16).

Table 1: The use of thermal networks for different conditions.

Phase	pole ≤ 3	pole > 3
> -55°~-45°	all	prefer nodal, recursive or Cauer-type recursive
< -55°~-45°	only Foster, Cauer or Cauer-recursive	

References

[1] M. Chen et al., "Narrow Band Internet of Things," IEEE Access, vol. 5, pp. 20557-20577, 2017.

[2] J. Ko et al., "Wireless Sensor Networks for Healthcare," Proc. of the IEEE, vol. 98, no. 11, pp. 1947-1960, 2010.

[3] S. K. Reynolds et al., "Design and Compliance Testing of a SiGe WCDMA Receiver IC With Integrated Analog Baseband," Proc. of the IEEE, vol. 93, no. 9, pp. 1624-1636, 2005.

[4] M. Schroter and A. Chakravorty, "Compact hierarchical modeling of bipolar transistors with HICUM," World Scientific, Singapore, 2010.

[5] G. Niu et al., MEXTRAM release 505.00, http://www.eng.auburn.edu/~niuguof/mextram/index.html, 2020.

[6] VBIC release 1.2, https://designers-guide.org/vbic/, 2020.

[7] A. K. Sahoo et al., "Thermal Impedance Modeling of Si–Ge HBTs From Low-Frequency Small-Signal Measurements," IEEE Electron Dev. Lett., vol. 32, no. 2, pp. 119-121, 2011.

[8] A. K. Sahoo et al., "A Geometry Scalable Model for Nonlinear Thermal Impedance of Trench Isolated HBTs," IEEE Electron Dev. Lett., vol. 36, no. 1, pp. 56-58, 2015.

[9] M. Couret et al., "Physical, small-signal and pulsed thermal impedance characterization of multi-finger SiGe HBTs close to the SOA edges," IEEE 32nd Int'l Conference on Microelectronic Test Structures (ICMTS), pp. 154-159, 2019.

[10] B. Heinemann et al., "SiGe HBT Technology with f_T/f_{max} of 300 GHz/500 GHz and 2.0 ps CML Gate Delay," IEEE IEDM Techn. Dig., pp. 688-691, 2010.

[11] C. Weimer, "DMT-pylab - A Python based measurement instruments remote control framework," Private project, 2021.

[12] K. Lu and X. Zhang, "Characterization and modeling of thermal dynamic behavior of AlGaAs/GaAs HBTs," IEEE MTT-S Int'l Microw. Symp., pp. 611-614 vol.2, 1998.

[13] N. Rinaldi, "Small-signal operation of semiconductor devices including self-heating, with application to thermal characterization and instability analysis," IEEE Trans. on Electron Dev., vol. 48, no. 2, pp. 323-331, 2001.

[14] G. Liang, "Investigation on temperature dependence of thermal constant and thermal impedance of SiGe HBT," Studienarbeit, Technische Universität Dresden, 2021.

[15] J. A. Lonac et al., "A simple technique for measuring the thermal impedance and the thermal resistance of HBTs," Europ. Gallium Arsenide and Other Semiconductor Application Symp., pp. 197-200, 2005.

[16] Z. Zhou et al., "Compact thermal model of a three-phase IGBT inverter power module," 26th Int'l Conference on Microelectronics, pp. 167-170, 2008.

[17] A. K. Sahoo et al., "Thermal Impedance Modeling of Si–Ge HBTs From Low-Frequency Small-Signal Measurements," IEEE Electron Dev. Lett., vol. 32, no. 2, pp. 119-121, 2011.

[18] Y. Zimmermann, "Contributions to the Analytical Modeling of Distributed Thermal and Electrical Substate Coupling Effects in Heterojunction Bipolar Transistors," PhD diss., TUDPress, 2017.

[19] A. Sahoo, "Electro-thermal characterizations, compact modeling and TCAD based device simulations of advanced SiGe: C BiCMOS HBTs and of nanometric CMOS FET," PhD diss., Université Bordeaux 1 Sciences et Technologie, 2012.

[20] A. K. Sahoo et al., "Electro-thermal characterization of Si-Ge HBTs with pulse measurement and transient simulation," Proc. of the Europ. Solid-State Dev. Research Conference, pp. 239-242, 2011.